Structural and Dynamic Features of the MutT Protein in the Recognition of Nucleotides with the Mutagenic 8-Oxoguanine Base*⒮

Teruya Nakamura[‡], **Sachiko Meshitsuka**[§], **Seiju Kitagawa**[§], **Nanase Abe**[§], **Junichi Yamada**[§], **Tetsuya Ishino**[§], **Hiroaki Nakano**[§], **Teruhisa Tsuzuki**[¶], **Takefumi Doi**[§], **Yuji Kobayashi**[§], **Satoshi Fujii**[‖], **Mutsuo Sekiguchi**[**], and **Yuriko Yamagata**[‡1]

From the [‡]Graduate School of Pharmaceutical Sciences, Kumamoto University, Kumamoto 862-0973, the [§]Graduate School of Pharmaceutical Sciences, Osaka University, Suita 565-0871, the [¶]Graduate School of Medical Sciences, Kyushu University, Fukuoka 812-8582, the [‖]School of Pharmaceutical Sciences, University of Shizuoka, Shizuoka 422-8526, and the [**]Fukuoka Dental College, Fukuoka 814-0193, Japan

Escherichia coli **MutT hydrolyzes 8-oxo-dGTP to 8-oxo-dGMP, an event that can prevent the misincorporation of 8-oxoguanine opposite adenine in DNA. Of the several enzymes that recognize 8-oxoguanine, MutT exhibits high substrate specificity for 8-oxoguanine nucleotides; however, the structural basis for this specificity is unknown. The crystal structures of MutT in the apo and holo forms and in the binary and ternary forms complexed with the product 8-oxo-dGMP and 8-oxo-dGMP plus Mn^{2+}, respectively, were determined. MutT strictly recognizes the overall conformation of 8-oxo-dGMP through a number of hydrogen bonds. This recognition mode revealed that 8-oxoguanine nucleotides are discriminated from guanine nucleotides by not only the hydrogen bond between the N7-H and Oδ (N119) atoms but also by the *syn* glycosidic conformation that 8-oxoguanine nucleotides prefer. Nevertheless, these discrimination factors cannot by themselves explain the roughly 34,000-fold difference between the affinity of MutT for 8-oxo-dGMP and dGMP. When the binary complex of MutT with 8-oxo-dGMP is compared with the ligand-free form, ordering and considerable movement of the flexible loops surrounding 8-oxo-dGMP in the binary complex are observed. These results indicate that MutT specifically recognizes 8-oxoguanine nucleotides by the ligand-induced conformational change.**

Although spontaneous mutations are indispensable to the evolutionary process of living organisms, they can also be lethal to the organism. Among the various modified bases in DNA,

RNA, and nucleotides, 8-oxoguanine (8-oxoG),[2] a damaged form of guanine (G) generated by reactive oxygen species, is known to have highly mutagenic potency because of its mispairing with adenine. Therefore, organisms have an error avoidance pathway for preventing mutations caused by 8-oxoG. The *Escherichia coli* MutT protein (129 amino acids, $M_r = 14,900$) hydrolyzes 8-oxo-dGTP and 8-oxo-GTP to their corresponding nucleoside monophosphates and inorganic pyrophosphate in the presence of Mg^{2+} (1, 2). Because 8-oxo-dGTP and 8-oxo-GTP can be misincorporated opposite adenine by DNA and RNA polymerases, the hydrolysis of the damaged nucleotides by MutT can avoid replicational and transcriptional errors. In DNA, 8-oxoG paired with cytosine is excised by MutM, an 8-oxoG DNA glycosylase, whereas MutY, an adenine DNA glycosylase, removes adenine paired with 8-oxoG (3–6).

The substrate specificities of enzymes that recognize 8-oxoG are quite varied. MutT exhibits high substrate specificity for 8-oxoG nucleotides; that is, the K_m for 8-oxo-dGTP is 14,000-fold lower than that for dGTP (7). In contrast, human MutT homologue 1 (hMTH1) hydrolyzes not only 8-oxo-dGTP but also several oxidized purine nucleotides such as 2-oxo-dATP, 2-oxo-ATP, 8-oxo-dATP, and 8-oxo-ATP. In terms of the hydrolysis of 8-oxo-dGTP, the K_m of hMTH1 for 8-oxo-dGTP is only 17-fold lower than that for dGTP (8, 9). The solution structure of hMTH1 as determined by NMR has revealed its overall architecture and possible substrate-binding region (10); however, the broad substrate recognition mechanism of hMTH1 remains to be elucidated. MutM and MutY also have low specificity for 8-oxoG. For example, MutM can recognize a variety of damaged bases such as formamidopyrimidine, 5-hydroxycytosine, and dihydrouracil in addition to 8-oxoG (11–13), and MutY shows a kinetic preference for A:8-oxoG that is only 6-fold greater than that for A:G (14).

The crystal structures of OGG1, MutM, and MutY complexed with 8-oxoG-containing DNA (13, 15, 16) have revealed

⒮ The on-line version of this article (available at http://www.jbc.org) contains supplemental Figs. S1–S4.
The atomic coordinates and structure factors (codes 3A6S, 3A6T, 3A6U, and 3A6V) have been deposited in the Protein Data Bank, Research Collaboratory for Structural Bioinformatics, Rutgers University, New Brunswick, NJ (http://www.rcsb.org/).
[1] To whom correspondence should be addressed: Graduate School of Pharmaceutical Sciences, Kumamoto University, 5-1 Oe-honmachi, Kumamoto 862-0973, Japan. Tel./Fax: 81-96-371-4638; E-mail: yamagata@gpo.kumamoto-u.ac.jp.

[2] The abbreviations used are: 8-oxoG, 8-oxoguanine; Nudix, nucleoside diphosphate linked to some other moiety, *X*; SLHL, strand-loop-helix-loop; r.m.s.d., root mean square deviation; AMPCPP, adenosine 5′-(α,β-methylenetriphosphate); SeMet, selenomethionine; hMTH1, human MutT homologue 1.

that, interestingly, OGG1 and MutM do not recognize the O8 atom, which is the most characteristic feature of the 8-oxoG moiety, and the interaction observed between the O8 atom and the main-chain atom of MutY is relatively weak. Alternatively, OGG1, MutM, and MutY commonly discriminate 8-oxoG from G by the protonation at N7 accompanied by the oxidation of C8. Structural studies on various enzymes that recognize 8-oxoG have succeeded in explaining the mechanism by which 8-oxoG is discriminated from normal G in DNA, but one of the most interesting questions to be elucidated is the mechanism by which MutT acquires extremely high substrate specificity for 8-oxoG compared with the other enzymes.

MutT belongs to the Nudix (nucleoside diphosphate linked to some other moiety, X) hydrolase family (17). Nudix family members have a highly conserved MutT signature (Nudix motif); *i.e.* $GX_5EX_7REUXEEXGU$, where U is a hydrophobic residue and *X* is any amino acid. Current genome analyses have found a large number of open reading frames containing the MutT signature, but their functions, *i.e.* their substrates, are not identified in the case of almost all these proteins because of a lack of homology outside the MutT signature. MutT is the most examined protein in this family. Its structure was first determined by NMR (18) and has greatly contributed to the study of the Nudix hydrolase family. NMR studies of MutT with its product, 8-oxo-dGMP, have predicted several recognition models of 8-oxo-dGMP (19). However, the precise recognition mechanism of 8-oxoG nucleotides remains unclear. Therefore, it is necessary to determine the crystal structures of MutT to explain the extremely high substrate specificity of MutT for 8-oxoG nucleotides.

Here, we present x-ray crystallographic analyses of the apo enzyme; the Mn^{2+}-bound holo enzyme (MutT-Mn^{2+}); the binary complex with 8-oxo-dGMP, a reaction product (MutT-8-oxo-dGMP); and the tertiary complex with 8-oxo-dGMP and Mn^{2+} (MutT-8-oxo-dGMP-Mn^{2+}). These structures have revealed the mechanism of the extremely high substrate specificity of MutT for 8-oxoG nucleotides and have allowed us to propose the exact roles of some conserved residues in the MutT signature.

EXPERIMENTAL PROCEDURES

Protein Expression and Purification—The *E. coli* strain BL21 (DE3) harboring a newly constructed pET8c/MutT plasmid was used for the expression of native and selenomethionine (SeMet)-substituted MutTs. Native MutT was overexpressed in Luria-Bertani (LB) broth, and SeMet MutT was overexpressed in LeMaster broth containing seleno-DL-methionine instead of methionine with sufficient amounts of isoleucine, lysine, and threonine to inhibit the methionine pathway (20, 21). This condition was also present in the overexpression of SeMet hMTH1 (22). Purification of MutT was carried out by almost the same procedure (except that the hydroxyapatite column chromatography step was skipped), as described previously (23). DEAE-Sepharose and the HiPrep 16/60 Sephacryl S-200 HR column were substituted for DEAE-Sephacel and the Sephadex G-75 column, respectively. The purified protein solution was concentrated to ~6 mg/ml.

Crystallization—The native and SeMet-substituted apo forms and all complexes were crystallized by hanging drop vapor diffusion at 288 K. Crystals of native and SeMet-substituted forms were obtained from a droplet containing 3 mg/ml protein, 10 mM Tris-HCl (pH 7.5), 0.5 mM EDTA, 2.5% glycerol, 0.5 mM 2-mercaptoethanol, 0.7 M potassium sodium tartrate, and 44 mM HEPES-NaOH (pH 7.5) equilibrated against a reservoir containing 1.4 M potassium sodium tartrate and 87 mM HEPES-NaOH (pH 7.5). Crystals of MutT-Mn^{2+} were obtained in the same manner, as described above, except that 10 mM $MnCl_2$ was added to the droplet. The crystallizations of MutT-8-oxo-dGMP and MutT-8-oxo-dGMP-Mn^{2+} were described previously (24). The crystals were transferred to a cryosolution of each reservoir containing 30% sucrose and were then flash frozen.

Data Collection, Processing, Phasing, and Structure Refinement—Diffraction data were collected at 100 K on beamline 18B of the Photon Factory (Tsukuba, Japan) and on beamlines 41XU, 44XU, 38B1, and 40B2 of SPring-8 (Harima, Japan). The data for native and SeMet derivative forms were processed and scaled by DSP/MOSFLM and SCALA (25). The data for MutT-Mn^{2+} were processed and scaled by DENZO and SCALEPACK (26). There are two molecules in the asymmetric unit with V_M of 2.2 (native MutT) and 2.5 (MutT-Mn^{2+}) $Å^3·Da^{-1}$ (27). Data collection statistics of the best data used for structure determination and refinements are listed in Table 1. Data collection statistics of MutT-8-oxo-dGMP and MutT-8-oxo-dGMP-Mn^{2+} are quoted from the reference by Nakamura *et al.* (24).

The positions of eight selenium atoms were determined using SOLVE (28). The initial phases were calculated using MLPHARE (29) and improved using DM (30). The initial model was built using TOM (31) and O (32). The model was refined using X-PLOR (33) and CNS (34). Using the model of the SeMet derivative, the successive refinement of native MutT converged at an R value of 20.4% and an R_{free} of 23.1% for reflections in the resolution range 20–1.8 Å. The structure of MutT-8-oxo-dGMP was solved by molecular replacement with AMoRe (35) using the structure of the native apo form as a search model. The $2F_o - F_c$ maps after CNS refinements clearly showed the density for 8-oxo-dGMP and the conformationally changed loop regions (L-A and L-D). These regions were manually built and fitted into the density with O. The structure of MutT-8-oxo-dGMP-Mn^{2+} was refined starting with the coordinates of the MutT-8-oxo-dGMP. The structure of MutT-Mn^{2+} was solved by molecular replacement with AMoRe by using the structure of the apo form as a search model. The stereochemical qualities of the structures were checked by PROCHECK (36); the refinement statistics are listed in Table 2. Superposition of MutT structures were carried out using Lsqkab (37). All molecular graphics were prepared using PyMOL (38).

RESULTS AND DISCUSSION

Overall Structures of MutT and MutT-8-oxo-dGMP—The crystal structures of the MutT apo and MutT-8-oxo-dGMP complex forms were determined at a resolution of 1.8 and 1.96 Å, respectively. MutT is composed of two α-helices (α-1 and α-2) and six β-strands (β-1 to β-6) (Figs. 1 and 2*A*); it adopts an

TABLE 1

Data collection statistics

Values in parentheses correspond to the highest resolution shell.

Diffraction data	MutT				MutT–8-oxo-dGMP	MutT–8-oxo-dGMP–Mn²⁺
	Native	Peak	Edge	Remote		
Beam line	SPring-8 BL41XU		PF BL18B		SPring-8 BL41XU	SPring-8 BL40B2
Wavelength (Å)	0.7080	0.9793	0.9791	0.9500	0.9000	1.296
Space group	$P2_1$		$P2_1$		$P2_12_12_1$	$P2_12_12_1$
Unit-cell lengths (Å, °)	$a = 33.9$		$a = 34.1$		$a = 37.9$	$a = 38.2$
	$b = 71.6$		$b = 71.1$		$b = 56.0$	$b = 56.0$
	$c = 55.8$		$c = 55.7$		$c = 59.4$	$c = 59.3$
	$\beta = 99.0$		$\beta = 98.7$			
Resolution range (Å)	20.0–1.8 (1.9–1.8)		20.0–2.2 (2.3–2.2)		20.0–1.96 (2.08–1.96)	18.56–2.56 (2.72–2.56)
No. of observed reflections	85,618	49,308	49,226	50,094	54,195	26,502
No. of unique reflections	24,217	13,041	13,015	13,147	9,344	4,395
Completeness (%)	99.7 (99.7)	97.2 (97.2)	97.3 (97.3)	98.3 (98.3)	97.6 (93.2)	99.2 (95.7)
$R_{merge}{}^{a}$ (%)	3.1 (9.4)	3.9 (12.1)	3.8 (12.3)	3.9 (12.1)	6.5 (18.1)	7.7 (15.2)
$\langle I/\sigma \rangle$	15.8 (7.9)	8.8 (3.3)	9.4 (5.0)	8.8 (5.6)	29.6 (6.2)	45.9 (22.6)

	MutT-Mn²⁺
Beam line	PF BL18B
Wavelength (Å)	1.000
Space group	$P2_1$
Unit-cell lengths (Å, °)	$a = 35.8$
	$b = 56.0$
	$c = 74.1$
	$\beta = 96.4$
Resolution range (Å)	40.0–2.0 (2.03–2.00)
No. of observed reflections	77,213
No. of unique reflections	19,810
Completeness (%)	98.1 (96.2)
$R_{merge}{}^{a}$ (%)	4.2 (6.4)
$\langle I/\sigma \rangle$	28.6 (18.6)

$^a R_{merge} = 100 \times \Sigma |I_{hkl} - \langle I_{hkl} \rangle| / \Sigma I_{hkl}$, $\langle I_{hkl} \rangle$ is the mean value of I_{hkl}.

TABLE 2

Refinement statistics

Diffraction data	MutT	MutT–8-oxo-dGMP	MutT–8-oxo-dGMP–Mn²⁺	MutT-Mn²⁺
Resolution range (Å)	20.0–1.8	20.0–1.96	18.56–2.56	20.0–2.0
Number of reflections used	24,213	9,280	4,394	19,386
Number of atoms				
Protein	2,025	1,038	1,029	2,010
Water	190	136	92	131
Nucleotide	0	24	24	0
Mn²⁺ ion	0	0	1	4^a
Other	11	34	5	32
Completeness (%)	99.1	97.3	99.9	98.1
$R_{cryst}/R_{free}{}^{b}$ (%)	20.4/23.1	17.8/20.1	19.3/24.2	19.2/22.7
Ramachandran plot (%)				
Most favored	93.0	91.5	87.6	94.9
Additional allowed	7.0	8.5	12.4	5.1
Generously allowed	0	0	0	0
Disallowed	0	0	0	0
r.m.s.d. in bonds (Å)	0.005	0.005	0.007	0.005
r.m.s.d. in angles (°)	1.2	1.3	1.3	1.2

^{a} Two ions per monomer.
$^b R_{cryst} = 100 \times \Sigma ||F_o| - |F_c|| / \Sigma |F_o|$. R_{free} was calculated from the test set (5% of the total data).

α-β-α sandwich structure that is conserved among members of the Nudix family. The Nudix motif (23 residues from Gly-38 *i.e.* the MutT signature ($GX_5EX_7REUXEEXGU$), adopts the characteristic strand-loop-helix-loop (SLHL) structure formed by β-3′, L-B, α-1, and L-C (39, 40). The crystal of the apo form contains two protein molecules per asymmetric unit, and they are very similar to each other with root mean square deviation (r.m.s.d.) of 0.5 Å for the corresponding 121 Cα atoms. For simplicity, only one molecule will be referred to in all further discussions. MutT exists as a monomer, which is found in the MutT-8-oxo-dGMP crystal.

In the apo form, the electron densities of L-A connecting β-2 and β-3 are not available, indicating that the L-A loop region has a highly flexible conformation (Fig. 2*A*). On the other hand, in the MutT-8-oxo-dGMP complex, the ordering of the flexible L-A loop by interactions with 8-oxo-dGMP was observed (Fig. 2, *B* and *C*). The plot of the displacement between the Cα atoms of the apo and complex forms is shown in supplemental Fig. S1A. The movements of the L-A and L-D regions are large (~8–10 Å) (Fig. 2*C* and supplemental Fig. S1A). Except for these loop regions, the two forms have a similar structure with an r.m.s.d. of 0.9 Å for the corresponding 101 Cα atoms.

A structural similarity search performed using the DALI server (41), with the coordinates of MutT-8-oxo-dGMP, indicated that 62 proteins (154 Protein Data Bank (PDB) ID numbers, 278 protein chains) are structural homologs of MutT with Z-scores of >6.0 and belong to the Nudix superfamily with the Nudix fold. The MutT structure, with two α-helices and six β-strands, comprises the smallest structural unit among members of the Nudix superfamily. Of 62 proteins, half have

β-1   β-2   β-3 β-3'   α-1   β-4

```
                          1                                                                                     77
E.coli              ---MKKLQIAVGIIRNE-------NNEIFITRRAA-----DAHMANKLEFPGGKIEMGETPEQAVVRELQEEVGITPQHFSLFEKLYEFPD
Y.pestis            ---MKHLQIAVGIIRNS-------QQEIFITQRAA-----DSHMAGFWEFPGGKIEQGETPEIALKRELLEETGIVVQQATLLTMLEHTFSD
P.mirabilis(37-164) ---KKKLHIAAGVICDK-------QNNVFITQRPL-----TSHMGGYWEFPGGKLEDKETPEQALYRELQEEIGINVTQCQLLETVEHDFID
P.rustigianii       -MEKKHLHIAAGIIRTA-------QQHIFITQRPE-----GTHMAGFWEFPGGKLPEDALIRELEEEIGIIVTDCSLFHRVDHEFDD
V.cholerae          ---MKRIHIVAGIIFNSD------QSEIFITKRPD-----HLHKGGFWEFPGGKVEAGESREQAMVRELEEEIGITVTEQQAFQHFDFDYTD
P.aeruginosa(1-136) ---MKRVHVAAAVIRGS-------DGRVLIARRPE-----DKHQGGLWEFPGGKVEDGEPVRAALARELEEELGIRVERARPLIQVRHDYAD
E.coli Orf135       ---MKMIEVVAAIIERD-------GKILLAQRPA-----QSDQAGLWEFPGGKVEPDESQRQALVRELREELGIEATVGEYVASHQREVSG
human MTH1(1-137)   ---MGASRLYTLVLVLQ-------PQRVLLGMKKR------GFGAGRWNGFGGKVQEGETIEDGARRELQESGLTVDALHKVGQIVFEFVG
B.subtilis YtkD     MYEFKDYYQNTVQLSFDDQPFSDSPKHVWVICRFGGKWLLTEHEDRGYEFGGKVEPMECAEEAALRELKEETGARVKSLKYLGQYKVLGKE
```

└ MutT signature ┘
(Nudix motif)

β-5   β-6   α-2

```
                    78                                                    129
E.coli              R--HITLWFWLVERWEGEPWGKEGQ-PGEWMSLVG----LNADDFPPANEPVIAKLKRL-------
Y.pestis            R--IVTLHFYRVEVWDGEPFGREGQ-PMRWVLQSE----LRADEFPPANAAIIELLTK--------
P.mirabilis(38-164) R--HITLSFFLVTEWENKPYGKEGQ-LSRWIPIMS----LNAEDFPPANRSIVALLQK--------
P.rustigianii       R--FITLYFMVSDWRNEPYGREGD----LIADEFPPANRVIVDMLTKAV-------
V.cholerae          K--SLSFDFMLVTAFDGQPHGREGQ-QGGWVKIAD----LANYRFPEANDPVVKQVIAQFG-----
P.aeruginosa(1-136) K--HVLLDVWEVDGFSGEAHGAEGQ-PLAWVEPRE----LADYEFPAANAPIVQAARLPAHYLITP
E.coli Orf135       R--IIHLHAWHVPDFHGTLQAHEHQ-ALVWCSPEE----ALQYPLAPADIPLLEAFMALRAARPAD
human MTH1(1-137)   EPELMDVHVFCTDSIQGTPVESDEM-RPCWFQLDQ----IPFKDMWPDDSYWFPLLLQKKKFHGYI
B.subtilis YtkD     KVIVKNIYFADIELKEKQADYFETKGPVLFHELPENLSRNKKFSFIMKDSVLPISLKKLKESGWIE
```
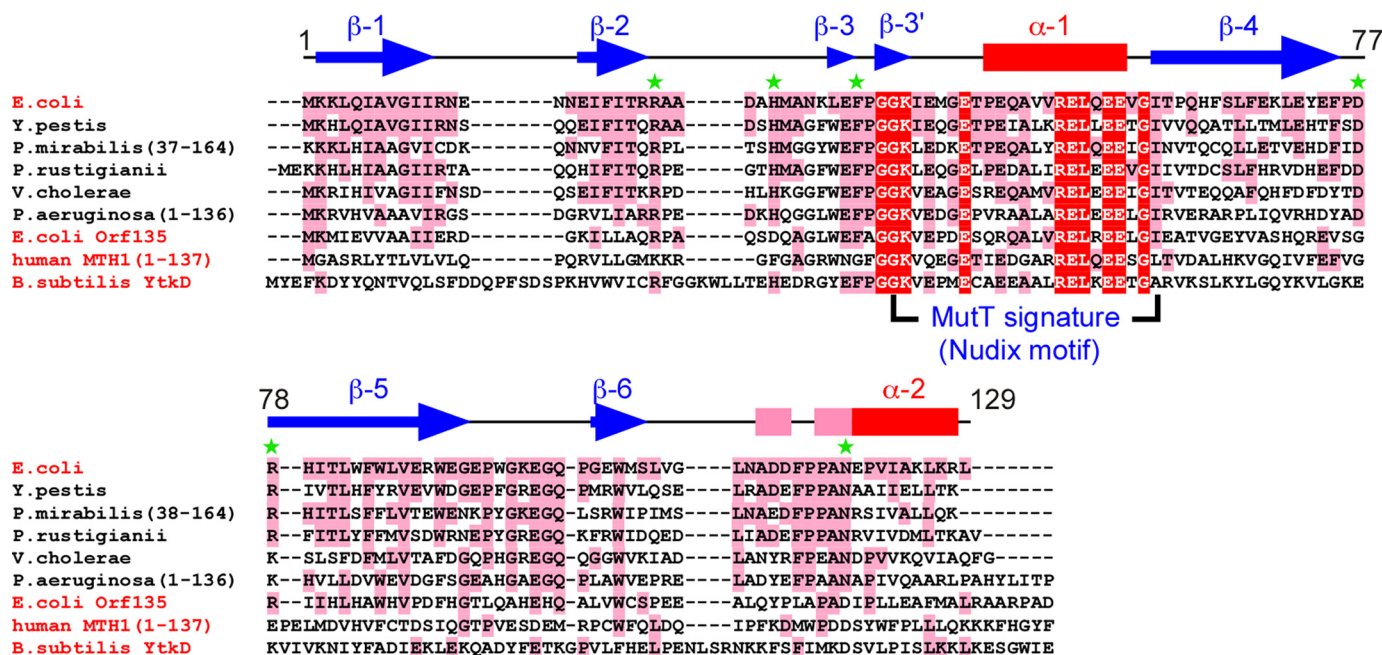
FIGURE 1. **Sequence alignment of MutT family proteins.** Amino acid sequences of MutT family proteins were aligned using ClustalW (72). MutT homologs from species related to *E. coli*, which share high sequence similarity, were chosen and are listed. They are from *E. coli* (CAA28523), *Yersinia pestis* (NP_670913), *Proteus mirabilis* (ZP_03840798), *Providencia rustigianii* (ZP_03315124), *Vibrio cholerae* (NP_232022), and *Pseudomonas aeruginosa* (ZP_04932260). In addition to *E. coli* MutT, *E. coli* Orf135 (BAA15549), human MTH1 (BAA07601), and *B. subtilis* YtkD (NP_390941), which have 8-oxo-dGTPase activity *in vitro*, were added and are shown in *red*. Absolutely conserved residues are shown in *red*, and identical residues are in *pink*. The *green asterisks* on the *E. coli* MutT sequence indicate amino residues that participate in the recognition of 8-oxoG and the ligand-induced conformational change. The secondary structure of *E. coli* MutT in the apo form is shown at the *top*. The α-helices, β-strands, and 3$_{10}$ helices are represented as *red bars*, *blue arrows*, and *pink bars*, respectively.

unknown functions. Structures that are highly similar to the MutT complex form are the monomer structures of *Bdellovibrio bacteriovorus* RNA pyrophosphohydrolase; *i.e.* BdRppH in the ternary and binary forms complexed with GTP and Mg^{2+} (BdRppH-GTP-Mg^{2+}, 3FFU, r.m.s.d. = 1.8 Å, Z = 19.0) and with dGTP (BdRppH-dGTP, 3EF5, r.m.s.d. = 1.9 Å, Z = 18.3) (40) and unknown proteins from *Bartonella henselae* (3HHJ, r.m.s.d. = 1.8 Å, Z = 19.8) and *Methanosarcina mazei* (3GRN, r.m.s.d. = 2.1 Å, Z = 17.5), respectively. In MutT, the r.m.s.d. is rather large: 3.3 Å for 120 Cα atoms between the x-ray and NMR structures in the ligand-free form and 3.5 Å for 127 Cα atoms between structures in the complex form (PDB IDs: 1MUT and 1PUS) (18, 19).

Recognition Scheme of 8-oxo-dGMP by MutT—When 8-oxo-dGMP binds to MutT, large ligand-induced conformational changes occur in the L-A and L-D regions, namely, the ordering of the flexible L-A loop and considerable movement of L-A and L-D to the surrounding 8-oxo-dGMP (Figs. 2*C* and 3*A*). The side chains of Arg-23 and His-28 on L-A form hydrogen-bonding interactions with phosphate and sugar moieties of 8-oxo-dGMP, respectively, whereas Arg-78 interacts with the sugar moiety through a water-mediated hydrogen bond. Asp-77 and Arg-78 make two hydrogen bonds between their side chains. The conformational change of the L-A and L-D regions also produces the water molecule-mediated interaction between His-28 and Asp-77 and the CH-π interaction between His-28 and Phe-75 (Fig. 3*A* and supplemental Fig. S2). Thus, the loops L-A and L-D connect to each other, resulting in the formation of a cave composed of β-1, β-3, β-3', β-5, and α-2 for substrate binding (Fig. 3*B*). 8-Oxo-dGMP is inserted deeply into the cave

in which the wall on one side is filled with hydrophobic residues (Leu-4, Ile-6, Val-8, Ile-80, and Leu-82), and the other side and bottom include some polar residues (Arg-23 and Asn-119). The 8-oxoG base and the deoxyribose are perfectly buried, and the phosphate group faces the solvents (Fig. 3*B*). The glycosidic conformation of 8-oxo-dGMP bound to MutT is *syn*. This fact is consistent with the first suggestion by Bessman *et al.* that MutT may recognize the *syn* conformation, because the 8-substituted purine nucleotides were better substrates compared with the normal purine nucleotides (42). The sugar ring puckering and the sugar-phosphate backbone conformation of 8-oxo-dGMP are C2'-*endo* and *gauche⁻-trans*, respectively. These conformations are generally observed in 8-substituted purine nucleosides and 5'-nucleotides (43).

These ligand-induced conformational changes result in the strict recognition of the overall structure of 8-oxo-dGMP by MutT through a number of hydrogen bonds (Fig. 3*C*). The characteristic features of the 8-oxoG base are the oxygen atom (O8) at C8 and the hydrogen atom (N7-H) at N7 accompanied by oxidation. MutT recognizes N7-H of 8-oxoG by a hydrogen bond with Oδ of Asn-119 (Fig. 3*C*, a *red dashed line*). The 8-oxoG base is also recognized by hydrogen bonds with Asn-119 and Phe-35; *i.e.* the Nδ of Asn-119 forms a hydrogen bond with O6 of 8-oxoG, and the main-chain atoms of Phe-35 participate in three types of hydrogen bonds with N2-H, N1-H, and O6. On the other hand, the O8 atom does not form hydrogen bonds with any amino acid residues, although it does participate in the weak C-H–O interaction with the phenyl ring C-H of Phe-75 (C–O distance, 3.4 Å) and the van der Waals interactions with the side-chain C-H moieties of Phe-75, Pro-116, Leu-
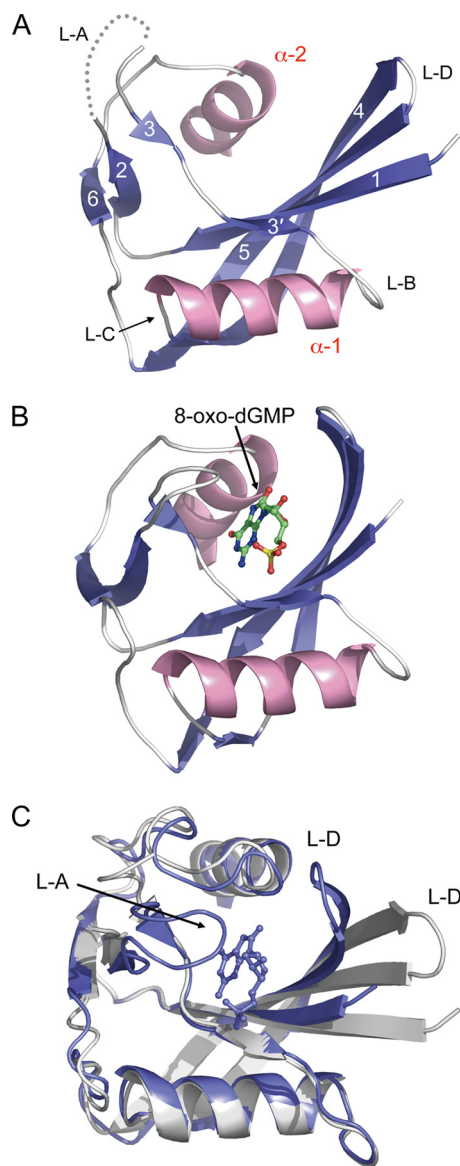
FIGURE 2. **Crystal structures of MutT apo and MutT-8-oxo-dGMP complex forms.** *A,* overall structure of MutT. α-Helices are in *pink,* and β-strands are in *slate.* A missing region of L-A is shown as a *gray dashed line. B,* overall structure of MutT-8-oxo-dGMP. 8-Oxo-dGMP is shown in *ball and stick representation. C,* comparison of the structures of the apo and complex forms. Apo and complex forms are shown in *gray* and *slate,* respectively. L-A and L-D regions in MutT-8-oxo-dGMP adopt a closed conformation as compared with those in the apo form.

82, Ile-80, and Ala-118 (Fig. 3*D*). In addition, the carbonyl oxygen of Gly-37 forms water molecule-mediated hydrogen bonds with N2-H of 8-oxoG and the phosphate oxygen. The side chain of His-28 is directly hydrogen-bonded to the O3′ atom of the deoxyribose. The O3′ atom also forms a hydrogen bond with a water molecule, binding to the side chain of Arg-78. The phosphate group forms a hydrogen bond with the side chain of Arg-23 and a water molecule-mediated hydrogen bond with the main chain of Lys-39. In summary, 8-oxo-dGMP is surrounded by 12 types of hydrogen bonds. The hydrogen-bonding interactions with the pyrimidine moiety and the α-phosphate group in MutT-8-oxo-dGMP are similar to those with the corresponding pyrimidine moieties and α-phosphate groups in the structures of BdRppH-GTP-Mg²⁺ and BdRppH-dGTP (BdRppH-

(d)GTPs) (40). The positions of the base moieties of (d)GTPs with the *syn* conformation in BdRppH-(d)GTPs accord with that of 8-oxo-dGMP in MutT-8-oxo-dGMP with an r.m.s.d. of 0.6 Å for the corresponding 11 atoms when proteins are superimposed. BdRppH with Arg-40, Phe-52, and Asn-136 residues corresponding to Arg-23, Phe-35, and Asn-119 of MutT, respectively, recognizes N1-H, N2-H, and O6 of the pyrimidine moiety by four hydrogen bonds with Phe-52 and Asn-136; Pα-O of the α-phosphate group is recognized by a hydrogen bond with Arg-40. This recognition mode is the same as that observed in MutT. Apart from the similarities, differences are found in recognition of the imidazole moiety of the base and the sugar moiety as well as in the ligand-induced conformational change. The imidazole and sugar moieties of (d)GTPs in BdRppH-(d)GTPs do not form hydrogen bonds with any residues in BdRppH. In addition, although ligand-induced conformational change with loop ordering is observed in BdRppH, the change is significantly small (~2–4 Å) as compared with that in MutT. The large ligand-induced conformational change observed in MutT does contribute to its high affinity for 8-oxoG nucleotides, as discussed below. There is a large discrepancy between the K_m values of 0.081 and 268 μM for the hydrolysis of 8-oxo-dGTP by MutT and of dGTP by BdRppH, respectively (7, 44). This may derive from these structural differences, in addition to the unfavorable *syn* conformation of (d)GTPs in BdRppH-(d)GTPs.

As a result of the strict recognition of 8-oxo-dGMP with the large conformational change, there are low *B* factors and unambiguous electron densities around 8-oxo-dGMP (supplemental Fig. S1*B* and Fig. 3*E*). The average *B* factor of 8-oxo-dGMP is 12.4 Å² and that of the residues involved in the recognition of 8-oxo-dGMP, Arg-23, His-28, Phe-35, Asp-77, Arg-78, and Asn-119 is 13.6 Å². These low *B* factors and unambiguous electron densities represent the small thermal motion and/or the ordered positioning of 8-oxo-dGMP and the residues of the active site in the crystal lattice. This phenomenon explains isothermal titration calorimetry experiments (45), indicating that the tight binding of 8-oxo-dGMP to MutT ($\Delta G = -9.8$ kcal/mol) is driven by a highly favorable enthalpy ($\Delta H = -39.0$ kcal/mol) with an unfavorable entropy ($-T\Delta S = 29.2$ kcal/mol). The unfavorable entropy would be a result of the conformational rigidity generated from the connection of loops L-A and L-D with large ligand-induced conformational changes. On the other hand, the more favorable enthalpy would be produced by the large number of hydrogen bonds and van der Waals interactions formed between 8-oxo-dGMP and MutT; this is sufficient to compensate for the unfavorable entropy and to bind tightly.

Furthermore, the hydrogen bond-mediated recognition mode found in MutT-8oxo-dGMP is comparable with the results of mutational studies in which it was found that the R78A, N119D, and N119A mutants show 7-, 37-, and 1650-fold decreases in affinity for 8-oxo-dGMP in comparison with the wild type and that they lose binding free energies ($\Delta\Delta G$) of 1.1, 2.1, and 4.3 kcal/mol, respectively, as measured by the increases in K_I (46). According to previous reports, the contribution of the hydrogen bond to protein stability can be estimated as ~2 and 1.2 kcal/mol for hydrogen bonds between protein residues
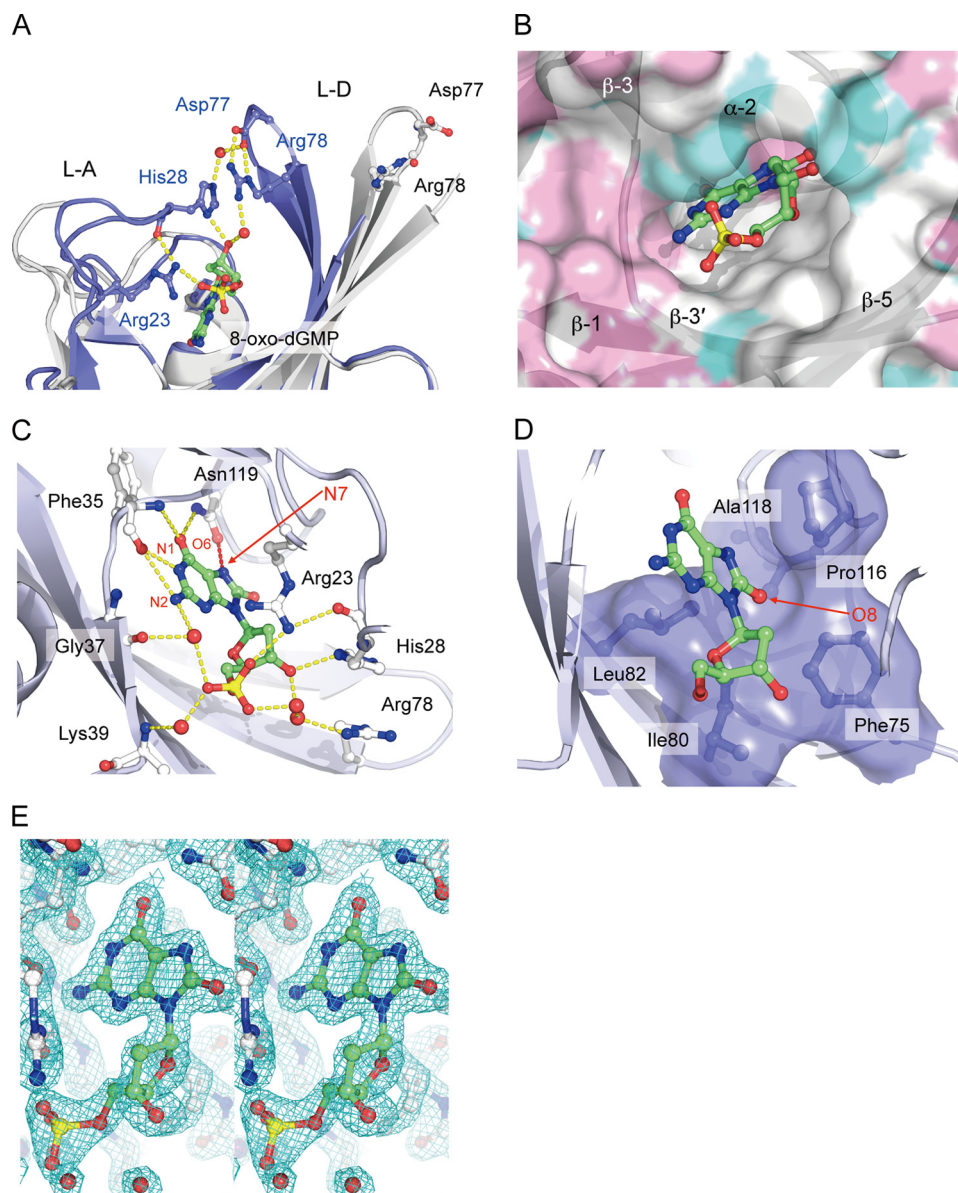
FIGURE 3. **Recognition of 8-oxo-dGMP by MutT.** *A*, hydrogen bonding interactions between 8-oxo-dGMP and loop regions (apo in *gray* and MutT-8-oxo-dGMP in *slate*). Amino acid residues involved in the hydrogen bonding interactions are shown in *ball and stick representation*. Water molecules are in *red*. Hydrogen bonds are shown as *yellow dashed lines*. *B*, the hydrophobic cave composed of *β*-1, *β*-3, *β*-3′, *β*-5, and *α*-2 is represented as a *translucent surface* (carbon in *white*, nitrogen in *cyan*, and oxygen in *pink*). *C*, interactions for the *syn* conformation of 8-oxo-dGMP. The hydrogen bond between Oδ of Asn-119 and N7-H of 8-oxoG is shown as a *red dashed line*. *D*, van der Waals interactions around the O8 atom. Amino acid residues recognizing O8 are shown in *ball, stick,* and *translucent surface*. *E*, a $2F_o - F_c$ electron density map around 8-oxo-dGMP contoured at 1.5 σ (*stereo view*).

both deoxyribose and ribose derivatives of 8-oxoG nucleotides with similar efficiency (2, 7). This is because, despite a number of hydrogen-bonding interactions between 8-oxo-dGMP and MutT, there is space for a hydroxyl group instead of the hydrogen atom at the 2′ position of the sugar ring (Fig. 3*B*). This recognition mechanism of 8-oxo-dGMP by MutT is different from any models predicted by NMR studies (PDB IDs: 1PPX, 1PUN, 1PUQ, 1PUS, and 1MUT) (supplemental Fig. S3).

Discrimination of 8-oxoG Nucleotides from G Nucleotides—The K_m values of *E. coli* MutT for 8-oxo-dGTP and 8-oxo-GTP are ~3,800- to 14,000-fold lower than the values for the corresponding G nucleotides (7). These data agree with the observation that the K_d value (52 nM) between 8-oxo-dGMP and MutT is 34,000-fold lower than that (1.76 mM) between dGMP and MutT (45). Thus, the most important question that this study addresses is the mechanism by which MutT obtains high substrate specificity for 8-oxoG nucleotides as compared with G nucleotides.

According to the recognition scheme of 8-oxo-dGMP by MutT, the major difference in the recognition of 8-oxoG *versus* G is whether the single hydrogen bond between Oδ of Asn-119 and N7-H of 8-oxoG occurs or not. This situation is similar to those of OGG1, MutM, and MutY (13, 15, 16). If the side-chain conformation of Asn-119 in the MutT complex with G nucleotides was the same as that in the MutT-8-oxo-dGMP structure, the two lone pairs at N7 of G and Oδ of Asn-119

and for those between a water molecule and a protein residue, respectively (47, 48). Judging from the MutT-8oxo-dGMP structure, the N119D and N119A mutants lose one hydrogen bond between the O6 of 8-oxo-dGMP and the Nδ-H of Asn-119 and two hydrogen bonds involving the O6 and N7-H of 8-oxodGMP and the amide group of Asn-119, respectively (Fig. 3*C*). The R78A mutant loses the hydrogen bond to a water molecule (Fig. 3*C*); that is, ΔΔ*G* losses of 1.2, 2, and 4 kcal/mol are estimated for the R78A, N119D, and N119A mutants, respectively; this agrees perfectly with the experimental data (46).

The feature of the substrate-binding site in MutT-8-oxo-dGMP is also consistent with reports that MutT hydrolyzes

would be repulsive (supplemental Fig. S4). To avoid this repulsion, a rotation about the side-chain torsion angles in Asn-119 should be required. Thus, the difference in the number of hydrogen bonds formed between MutT-G and MutT-8-oxoG complexes is only one. The contribution of one hydrogen bond to ΔΔ*G* is estimated to be 2 kcal/mol (47, 48).

The *syn* glycosidic conformation of 8-oxo-dGMP must also be one of the elements contributing to the substrate specificity of MutT, because 8-oxoG nucleotides favor a *syn* conformation by the steric hindrance between O8 and the sugar moiety; this is in contrast with G nucleotides that adopt both *syn* and *anti* conformations (49, 50). Because of the lack of quantitative data
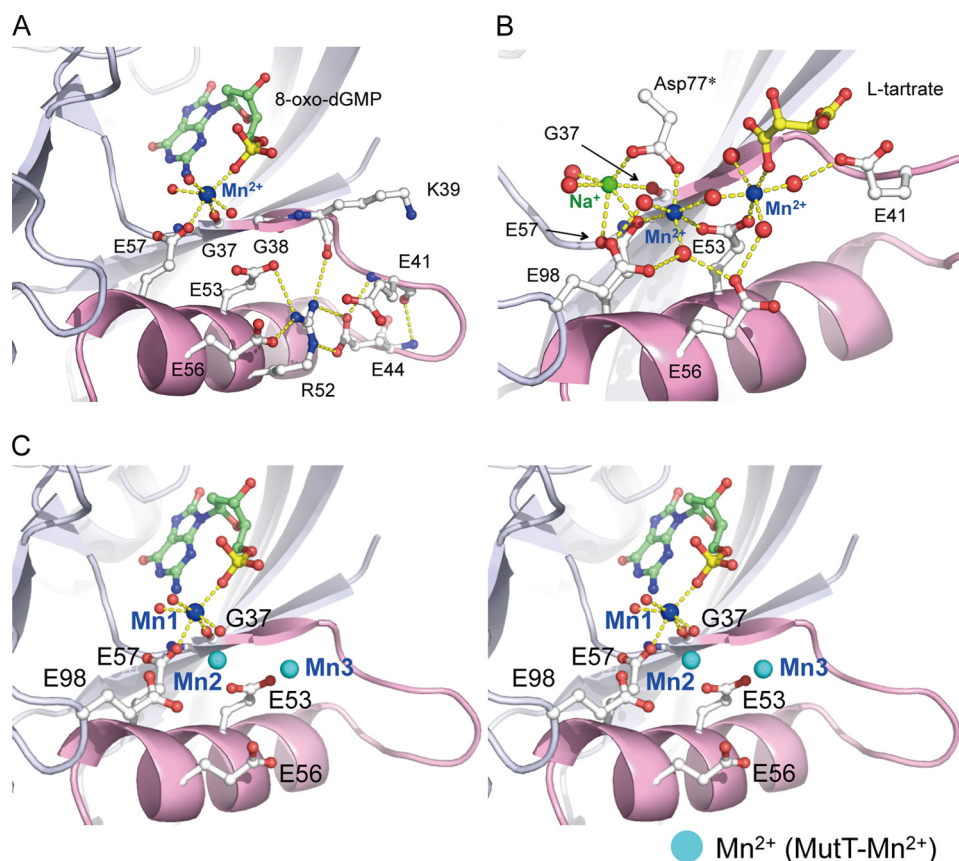
FIGURE 4. **Coordination scheme of Mn^{2+} at the MutT signature in MutT-8-oxo-dGMP-Mn^{2+} and MutT-Mn^{2+}.** *A*, the coordination scheme of Mn^{2+} and the structure of the MutT signature in MutT-8-oxo-dGMP-Mn^{2+}. Mn^{2+} in *blue* has an ideal octahedral coordination with Gly-37, Glu-57, Pα-O of 8-oxo-dGMP, and water molecules. The hydrogen bonding interactions shown in *yellow dashed lines* contribute to the conformational stabilization of the SLHL structure of the MutT signature. The SLHL structure is in *pink*. *B*, the coordination scheme of Mn^{2+} in MutT-Mn^{2+}. Na^+ is shown in *green*. Asp-77* is an amino acid of another molecule in the asymmetric unit. *C*, superposition of two Mn^{2+} ions in MutT-Mn^{2+} onto the structure of MutT-8-oxo-dGMP-Mn^{2+} (*stereo view*). *Coloring* is as in *A*. Mn^{2+} ions observed in MutT-Mn^{2+} are shown in *cyan* (*Mn2* and *Mn3*).

on the preference of the *syn* conformation about the 8-oxoG nucleotides, it is difficult to estimate the free energy difference between the *syn* and *anti* conformations. However, it is unlikely that the preference of MutT for the *syn* conformation over the *anti* conformation is more than 10-fold ($\Delta\Delta G \approx 1.4$ kcal/mol), because the *anti* conformation for 8-oxoG nucleotides is sometimes observed in the crystal structures of 8-oxoG recognition complexes such as OGG1 and MutY (15, 16).

These discrimination factors cannot by themselves explain the roughly 34,000-fold difference between the binding affinity of MutT for 8-oxo-dGMP and dGMP ($\Delta\Delta G \approx 6$ kcal/mol). When 8-oxo-dGMP binds to MutT, large ligand-induced conformational changes with an ordering of loop regions are observed. On the other hand, in the binding of dGMP to MutT, the thermal parameters were $\Delta G = -3.7$, $\Delta H = -3.3$, and $-T\Delta S = -0.4$ kcal/mol; the changes in backbone ^{15}N and NH chemical shifts in 22 residues; and the slowing down of the NH exchange with D_2O of 20 residues are remarkably different when compared with the changes (the thermal parameters of $\Delta G = -9.8$, $\Delta H = -39.0$, and $-T\Delta S = 29.2$ kcal/mol; the changes in backbone ^{15}N and NH chemical shifts in 62 residues; and the slowing down of the NH exchange with D_2O of 45 residues) involved in the binding of 8-oxo-dGMP to MutT (19,

45). These facts suggest that no significant conformational change in MutT is observed when dGMP binds to MutT. The large ligand-induced conformational change in MutT also contributes to the discrimination of 8-oxoG nucleotides from G nucleotides.

A comparison of the amino acid sequences of MutT-related enzymes suggests that the enzymes with higher substrate specificity for 8-oxoG are only MutT homologs from closely related species with conserved amino acids in the positions that participate in the recognition of 8-oxoG and the conformational change (Fig. 1, *green asterisk*). In fact, these amino acids are not highly conserved among *E. coli* Orf135 (51), *Bacillus subtilis* YtkD (52), and hMTH1 (8) that have broad substrate specificities.

Structure of the MutT Signature and Metal-binding Sites—We have solved two types of Mn^{2+}-bound structures, MutT-8-oxo-dGMP-Mn^{2+} and MutT-Mn^{2+}, to determine metal-binding sites at the MutT signature of MutT. The crystal of MutT-Mn^{2+} contains two proteins per asymmetric unit. Their overall structures are very similar, with an r.m.s.d. of 0.3 Å for the corresponding 118 Cα atoms; for sim-

plicity, only one molecule will be referred to in all further discussion. The structure of MutT-Mn^{2+} is similar to that of the apo form, with an r.m.s.d. of 0.6 Å for the corresponding 118 Cα atoms.

In the MutT signature having an SLHL structure (Fig. 4*A*), Gly-38, Glu-44, Arg-52, Glu-53, Glu-56, Glu-57, and Gly-59 are completely conserved among the members of the Nudix family (Fig. 1). The SLHL structure of MutT is similar to those of other enzymes in the Nudix family. For example, the conserved 23 residues can be superimposed on those found in the *Pyrobaculum aerophilum* Nudix protein with an r.m.s.d. of 0.5 Å (53). A characteristic feature in the SLHL structure is the hydrogen-bonding network centering on the converged Arg-52 that anchors α-1 to its connecting loop. The side chains of Glu-44 and Arg-52, which form two hydrogen bonds with each other, participate in hydrogen bonding to the main chain atoms in the nonconserved Glu-41 and Lys-39 residues, respectively. Arg-52 also interacts with the side chains of the conserved Glu-53 and Glu-56 residues (Fig. 4*A*). This hydrogen-bonding network is roughly the same as that in the other Nudix proteins and contributes to the conformational stability of the SLHL structure (39, 40, 53–65).

In the electron density maps of the MutT-Mn^{2+} crystal produced by co-crystallization, there were three peaks corresponding to the metal ions near the MutT signature. Judging from the peak heights, B factors, bond lengths, and bond angles, we determined that two peaks were Mn^{2+} ions (nearly ideal octahedral coordination and an average bond length of $\sim$2.2 Å) and one was Na^+ (distorted octahedral coordination and an average bond length of $\sim$2.5 Å) (Fig. 4*B*). Furthermore, the two Mn^{2+} sites were also confirmed from significant densities ($>$10 σ level) on the anomalous difference Fourier map at $\lambda = 1$ Å (data not shown). On the other hand, the densities of the Na^+ site were less than noise level. The refined MutT-Mn^{2+} structure reveals that two Mn^{2+} ions form a binuclear metal center with a bridged water molecule. One Mn^{2+} coordinates to the oxygen atoms of Glu-53, Glu-57, three water molecules, and Asp-77 in another molecule (Asp-77*). The coordination partners of another Mn^{2+} are Glu-53, L-tartrate (a crystallization reagent), and four water molecules. Na^+ coordinates to the oxygen atoms of Gly-37, Glu-57, Asp-77*, and two water molecules. Asp-77* and L-tartrate bind to the MutT signature through metal ions, but do not distort the SLHL structure.

In the MutT-8-oxo-dGMP-Mn^{2+} crystal (prepared by soaking MutT-8-oxo-dGMP crystals in reservoir supplemented with 1 mM $MnCl_2$), Mn^{2+} binds to the six oxygen atoms of the main chain of Gly-37, the side chain of Glu-57, the phosphate group, and three water molecules with nearly ideal octahedral coordination (Fig. 4*A*). The binding of Mn^{2+} to the MutT-8-oxo-dGMP binary complex makes the phosphate group move slightly toward Mn^{2+} (the P atom moves by 0.7 Å). The position of Mn^{2+} observed in MutT-8-oxo-dGMP-Mn^{2+} is close to that of Na^+ in MutT-Mn^{2+} (at a distance of 1.4 Å). The three Mn^{2+} binding sites consisting of the Mn^{2+} in MutT-8-oxo-dGMP-Mn^{2+} and two additional Mn^{2+} ions in MutT-Mn^{2+} (Fig. 4*C*) are located at common metal-binding sites observed in the Nudix family (60) and correspond to those observed in the ternary complexes of *E. coli* ADP-ribose pyrophosphatase, *Mycobacterium tuberculosis* ADP-ribose pyrophosphatase, *Caenorhabditis elegans* diadenosine $5',5'''-P^1,P^4$-tetraphosphate pyrophosphohydrolase, *Xenopus laevis* X29, human NUDT5, *Thermus thermophilus* Ndx2, and BdRppH (40, 55, 57, 64–67). Thus, the three sites are considered to be candidates for metal binding in 8-oxo-dGTP hydrolysis. Previous kinetic studies have shown that MutT binds to one Mn^{2+} in the absence of nucleotides and two Mn^{2+} ions in the presence of a nonspecific substrate analog, AMPCPP (68). The middle Mn^{2+} (*Mn2* in Fig. 4*C*) may be prebound to the active site, judging from the number of coordination partners in MutT and the Mn^{2+} ion (*Mn1* in Fig. 4*C*) found in MutT-8-oxo-dGMP-Mn^{2+}; otherwise, it and other Mn^{2+} ion (*Mn1* and *Mn3*, respectively in Fig. 4*C*) would be recruited with the substrate. The probability of the three metals binding to MutT in the presence of the real substrate 8-oxo-dGTP cannot be neglected because of the fact that the number of binding metals depends on the kinds of substrate analogs (40, 54, 60, 61, 64–66).

The structures of MutT-8-oxo-dGMP-Mn^{2+} and MutT-Mn^{2+} suggest structural insights into some essential or important residues for the 8-oxo-dGTP hydrolysis. Glu-53 and Glu-57 are essential for the suppression of spontaneous A:T to C:G transversion mutations (69), and E53Q and E57Q mutants decrease k_{cat} by 10^4 to 10^5-fold (70). On the other hand, Glu-56 is nonessential for the suppression of the mutations (69), and E56Q and E98Q mutants have relatively small effects ($<$24-fold) on k_{cat} (70). These results agree with our structural studies showing that essential residues, Glu-53 and Glu-57, directly bind to metal ions, whereas important residues, Glu-56 and Glu98, make water-mediated interactions with metal ions (Fig. 4, *A* and *B*). Gly-37 and Gly-38, which are located at the surface of the ligand-binding site, are also revealed to be essential residues for the suppression of the mutations (69). The side chains of any residues except Gly in positions 37 and 38 would contact the base moiety of the nucleotide ligand and the essential residue for the catalysis, Glu-53, respectively (Fig. 4, *A* and *C*). For this reason, to express 8-oxo-dGTPase activity, residues 37 and 38 must be Gly, which has the smallest side chain.

A number of kinetic, mutational, and NMR studies of MutT using dGTP and/or a substrate analog, AMPCPP, have been reported, and a catalytic mechanism is proposed by Mildvan and coworkers (71). Compared with our structural data, there appear to be some differences in the metal-binding sites. Gly-38 is involved in metal coordination in their model, but Gly-37, instead of Gly-38, is a metal ligand in the structure of MutT-8-oxo-dGMP-Mn^{2+} (Fig. 4, *A* and *C*). The all-crystal structures of Nudix proteins show that the carbonyl oxygen of the corresponding residue to Gly-38 participates in the formation of β-sheet, whereas that of Gly-37 binds to a metal ion (40, 55, 57–59, 61, 64–67). Glu-56 and Glu98, which are metal ligands in the model proposed by Mildvan and coworkers, interact with water molecules bound to metal ions in our structures. The metal coordination scheme changes in the active site during the reaction, and a more proper enzymatic mechanism activated by metal ions might be examined by kinetic protein crystallography.

REFERENCES

1. Maki, H., and Sekiguchi, M. (1992) *Nature* **355,** 273–275
2. Taddei, F., Hayakawa, H., Bouton, M., Cirinesi, A., Matic, I., Sekiguchi, M., and Radman, M. (1997) *Science* **278,** 128–130
3. Au, K. G., Cabrera, M., Miller, J. H., and Modrich, P. (1988) *Proc. Natl. Acad. Sci. U.S.A.* **85,** 9163–9166
4. Cabrera, M., Nghiem, Y., and Miller, J. H. (1988) *J. Bacteriol.* **170,** 5405–5407
5. Michaels, M. L., Cruz, C., Grollman, A. P., and Miller, J. H. (1992) *Proc. Natl. Acad. Sci. U.S.A.* **89,** 7022–7025
6. Tchou, J., Kasai, H., Shibutani, S., Chung, M. H., Laval, J., Grollman, A. P., and Nishimura, S. (1991) *Proc. Natl. Acad. Sci. U.S.A.* **88,** 4690–4694
7. Ito, R., Hayakawa, H., Sekiguchi, M., and Ishibashi, T. (2005) *Biochemistry* **44,** 6670–6674
8. Fujikawa, K., Kamiya, H., Yakushiji, H., Fujii, Y., Nakabeppu, Y., and Kasai, H. (1999) *J. Biol. Chem.* **274,** 18201–18205
9. Fujikawa, K., Kamiya, H., Yakushiji, H., Nakabeppu, Y., and Kasai, H. (2001) *Nucleic Acids Res.* **29,** 449–454
10. Mishima, M., Sakai, Y., Itoh, N., Kamiya, H., Furuichi, M., Takahashi, M., Yamagata, Y., Iwai, S., Nakabeppu, Y., and Shirakawa, M. (2004) *J. Biol. Chem.* **279,** 33806–33815
11. Tchou, J., Bodepudi, V., Shibutani, S., Antoshechkin, I., Miller, J., Grollman, A. P., and Johnson, F. (1994) *J. Biol. Chem.* **269,** 15318–15324
12. Hatahet, Z., Kow, Y. W., Purmal, A. A., Cunningham, R. P., and Wallace, S. S. (1994) *J. Biol. Chem.* **269,** 18814–18820
13. Fromme, J. C., and Verdine, G. L. (2003) *J. Biol. Chem.* **278,** 51543–51548
14. Porello, S. L., Leyes, A. E., and David, S. S. (1998) *Biochemistry* **37,**

14756–14764

15. Bruner, S. D., Norman, D. P., and Verdine, G. L. (2000) *Nature* **403,** 859–866

16. Fromme, J. C., Banerjee, A., Huang, S. J., and Verdine, G. L. (2004) *Nature* **427,** 652–656

17. Bessman, M. J., Frick, D. N., and O'Handley, S. F. (1996) *J. Biol. Chem.* **271,** 25059–25062

18. Abeygunawardana, C., Weber, D. J., Gittis, A. G., Frick, D. N., Lin, J., Miller, A. F., Bessman, M. J., and Mildvan, A. S. (1995) *Biochemistry* **34,** 14997–15005

19. Massiah, M. A., Saraswat, V., Azurmendi, H. F., and Mildvan, A. S. (2003) *Biochemistry* **42,** 10140–10154

20. Doublié, S. (1997) *Methods Enzymol.* **276,** 523–530

21. LeMaster, D. M., and Richards, F. M. (1985) *Biochemistry* **24,** 7263–7268

22. Nakamura, T., Kitaguchi, Y., Miyazawa, M., Kamiya, H., Toma, S., Ikemizu, S., Shirakawa, M., Nakabeppu, Y., and Yamagata, Y. (2006) *Acta Crystallogr. Sect. F Struct. Biol. Cryst. Commun.* **62,** 1283–1285

23. Akiyama, M., Maki, H., Sekiguchi, M., and Horiuchi, T. (1989) *Proc. Natl. Acad. Sci. U.S.A.* **86,** 3949–3952

24. Nakamura, T., Doi, T., Sekiguchi, M., and Yamagata, Y. (2004) *Acta Crystallogr. D Biol. Crystallogr.* **60,** 1641–1643

25. Rossmann, M. G., and van Beek, C. G. (1999) *Acta Crystallogr. D Biol. Crystallogr.* **55,** 1631–1640

26. Otwinowski, Z., and Minor, W. (1997) *Methods Enzymol.* **276,** 307–326

27. Matthews, B. W. (1968) *J. Mol. Biol.* **33,** 491–497

28. Terwilliger, T. C., and Berendzen, J. (1999) *Acta Crystallogr. D Biol. Crystallogr.* **55,** 849–861

29. Collaborative Computational Project, Number 4. (1994) *Acta Crystallogr. D Biol. Crystallogr.* **50,** 760–763

30. Cowtan, K. (1994) *Joint CCP4 and ESF-EACBM Newsletter on Protein Crystallography* **31,** 34–38

31. Cambillau, C., Horjales, E., and Jones, T. A. (1984) *J. Mol. Graph.* **2,** 53–54

32. Jones, T. A., Zou, J. Y., Cowan, S. W., and Kjeldgaard, M. (1991) *Acta Crystallogr. Sect. A* **47,** 110–119

33. Brünger, A. T. (1992) *A System for X-Ray Crystallography and NMR*, Yale University Press, New Haven, CT

34. Brünger, A. T., Adams, P. D., Clore, G. M., DeLano, W. L., Gros, P., Grosse-Kunstleve, R. W., Jiang, J. S., Kuszewski, J., Nilges, M., Pannu, N. S., Read, R. J., Rice, L. M., Simonson, T., and Warren, G. L. (1998) *Acta Crystallogr. D Biol. Crystallogr.* **54,** 905–921

35. Navaza, J. (1994) *Acta Crystallogr. Sect. A* **50,** 157–163

36. Laskowski, R. A., MacArthur, M. W., Moss, D. S., and Thornton, J. M. (1993) *J. Appl. Crystallogr.* **26,** 283–291

37. Kabsch, W. (1976) *Acta Crystallogr. Sect. A* **32,** 922–923

38. DeLano, W. L. (2002) *The PyMOL Molecular Graphics System*, DeLano Scientific LLC, San Carlos, CA

39. Gabelli, S. B., Bianchet, M. A., Xu, W., Dunn, C. A., Niu, Z. D., Amzel, L. M., and Bessman, M. J. (2007) *Structure* **15,** 1014–1022

40. Messing, S. A., Gabelli, S. B., Liu, Q., Celesnik, H., Belasco, J. G., Piñeiro, S. A., and Amzel, L. M. (2009) *Structure* **17,** 472–481

41. Holm, L., Kääriäinen, S., Rosenström, P., and Schenkel, A. (2008) *Bioinformatics* **24,** 2780–2781

42. Bhatnagar, S. K., Bullions, L. C., and Bessman, M. J. (1991) *J. Biol. Chem.* **266,** 9050–9054

43. Saenger, W. (1984) *Principles of Nucleic Acid Structure*, Springer-Verlag, New York

44. Steyert, S. R., Messing, S. A., Amzel, L. M., Gabelli, S. B., and Piñeiro, S. A. (2008) *J. Bacteriol.* **190,** 8215–8219

45. Saraswat, V., Massiah, M. A., Lopez, G., Amzel, L. M., and Mildvan, A. S. (2002) *Biochemistry* **41,** 15566–15577

46. Saraswat, V., Azurmendi, H. F., and Mildvan, A. S. (2004) *Biochemistry* **43,** 3404–3414

47. Funahashi, J., Takano, K., Yamagata, Y., and Yutani, K. (2002) *J. Biol. Chem.* **277,** 21792–21800

48. Takano, K., Yamagata, Y., Funahashi, J., Hioki, Y., Kuramitsu, S., and Yutani, K. (1999) *Biochemistry* **38,** 12698–12708

49. Kouchakdjian, M., Bodepudi, V., Shibutani, S., Eisenberg, M., Johnson, F., Grollman, A. P., and Patel, D. J. (1991) *Biochemistry* **30,** 1403–1412

50. Uesugi, S., Yano, J., Yano, E., and Ikehara, M. (1977) *J. Am. Chem. Soc.* **99,** 2313–2323

51. Kamiya, H., Murata-Kamiya, N., Iida, E., and Harashima, H. (2001) *Biochem. Biophys. Res. Commun.* **288,** 499–502

52. Xu, W., Jones, C. R., Dunn, C. A., and Bessman, M. J. (2004) *J. Bacteriol.* **186,** 8380–8384

53. Wang, S., Mura, C., Sawaya, M. R., Cascio, D., and Eisenberg, D. (2002) *Acta Crystallogr. D Biol. Crystallogr.* **58,** 571–578

54. Gabelli, S. B., Bianchet, M. A., Bessman, M. J., and Amzel, L. M. (2001) *Nat. Struct. Biol.* **8,** 467–472

55. Bailey, S., Sedelnikova, S. E., Blackburn, G. M., Abdelghany, H. M., Baker, P. J., McLennan, A. G., and Rafferty, J. B. (2002) *Structure* **10,** 589–600

56. Kang, L. W., Gabelli, S. B., Bianchet, M. A., Xu, W. L., Bessman, M. J., and Amzel, L. M. (2003) *J. Bacteriol.* **185,** 4110–4118

57. Kang, L. W., Gabelli, S. B., Cunningham, J. E., O'Handley, S. F., and Amzel, L. M. (2003) *Structure* **11,** 1015–1023

58. Shen, B. W., Perraud, A. L., Scharenberg, A., and Stoddard, B. L. (2003) *J. Mol. Biol.* **332,** 385–398

59. Gabelli, S. B., Bianchet, M. A., Azurmendi, H. F., Xia, Z., Sarawat, V., Mildvan, A. S., and Amzel, L. M. (2004) *Structure* **12,** 927–935

60. Ranatunga, W., Hill, E. E., Mooster, J. L., Holbrook, E. L., Schulze-Gahmen, U., Xu, W., Bessman, M. J., Brenner, S. E., and Holbrook, S. R. (2004) *J. Mol. Biol.* **339,** 103–116

61. Yoshiba, S., Ooga, T., Nakagawa, N., Shibata, T., Inoue, Y., Yokoyama, S., Kuramitsu, S., and Masui, R. (2004) *J. Biol. Chem.* **279,** 37163–37174

62. She, M., Decker, C. J., Chen, N., Tumati, S., Parker, R., and Song, H. (2006) *Nat. Struct. Mol. Biol.* **13,** 63–70

63. Zha, M., Zhong, C., Peng, Y., Hu, H., and Ding, J. (2006) *J. Mol. Biol.* **364,** 1021–1033

64. Scarsdale, J. N., Peculis, B. A., and Wright, H. T. (2006) *Structure* **14,** 331–343

65. Wakamatsu, T., Nakagawa, N., Kuramitsu, S., and Masui, R. (2008) *J. Bacteriol.* **190,** 1108–1117

66. Gabelli, S. B., Bianchet, M. A., Ohnishi, Y., Ichikawa, Y., Bessman, M. J., and Amzel, L. M. (2002) *Biochemistry* **41,** 9279–9285

67. Zha, M., Guo, Q., Zhang, Y., Yu, B., Ou, Y., Zhong, C., and Ding, J. (2008) *J. Mol. Biol.* **379,** 568–578

68. Frick, D. N., Weber, D. J., Gillespie, J. R., Bessman, M. J., and Mildvan, A. S. (1994) *J. Biol. Chem.* **269,** 1794–1803

69. Shimokawa, H., Fujii, Y., Furuichi, M., Sekiguchi, M., and Nakabeppu, Y. (2000) *Nucleic Acids Res.* **28,** 3240–3249

70. Harris, T. K., Wu, G., Massiah, M. A., and Mildvan, A. S. (2000) *Biochemistry* **39,** 1655–1674

71. Mildvan, A. S., Xia, Z., Azurmendi, H. F., Saraswat, V., Legler, P. M., Massiah, M. A., Gabelli, S. B., Bianchet, M. A., Kang, L. W., and Amzel, L. M. (2005) *Arch. Biochem. Biophys.* **433,** 129–143

72. Thompson, J. D., Higgins, D. G., and Gibson, T. J. (1994) *Nucleic Acids Res.* **22,** 4673–4680